

## A light NMSSM pseudoscalar Higgs boson at the LHC Run 2

N-E. Bomark<sup>a</sup>, S. Moretti<sup>b,\*</sup>, S. Munir<sup>c,d</sup>, and L. Roszkowski<sup>a,e</sup>

<sup>a</sup>National Centre for Nuclear Research, Hoża 69, 00-681 Warsaw, Poland

<sup>b</sup>School of Physics & Astronomy, University of Southampton, Southampton SO17 1BJ, UK

<sup>c</sup>Asia Pacific Center for Theoretical Physics, San 31,

Hyoja-dong, Nam-gu, Pohang 790-784, Republic of Korea

<sup>d</sup>Department of Physics and Astronomy, Uppsala University, Box 516, SE-751 20 Uppsala, Sweden and

<sup>e</sup>Department of Physics & Astronomy, University of Sheffield, Western Bank, Sheffield S10 2TN, UK

We revisit the light pseudoscalar  $A_1$  in the Next-to-Minimal Supersymmetric Standard Model (NMSSM) with partial universality at some high unification scale in order to delineate the parameter space regions consistent with up-to-date theoretical and experimental constraints and examine to what extent this state can be probed by the Large Hadron Collider (LHC) during Run 2. We find that it can be accessible through a variety of signatures proceeding via  $A_1 \rightarrow \tau^+\tau^-$  and/or  $b\bar{b}$ , the former assuming hadronic decays and the latter two  $b$ -tags within a fat jet or two separate slim ones. Herein, the light pseudoscalar state is produced from a heavy Higgs boson decay in either pairs or singly in association with a  $Z$  boson (in turn decaying into electrons/muons).

### I. INTRODUCTION

In this report we analyse in detail some of the processes that yield sizeable event rates and could potentially lead to the detection of a light  $A_1$  at the LHC with  $\sqrt{s} = 14$  TeV within the NMSSM [1]. We perform parameter scans of this scenario with partial universality at the Grand Unification Theory (GUT) scale to find regions where a light,  $\lesssim 150$  GeV,  $A_1$  can be obtained. In these scans we require the mass of the SM-like Higgs state discovered at the LHC, henceforth denoted by  $H_{\text{SM}}$ , to lie around 125 GeV and its signal rates in the  $\gamma\gamma$  and  $ZZ$  channels to be consistent with the SM expectations. We study in detail the two possibilities,  $H_{\text{SM}} = H_1$  and  $H_{\text{SM}} = H_2$ , as two separate cases. (Recall that the neutral Higgs spectrum of the NMSSM includes three CP-even states,  $H_{1,2,3}$ , and two CP-odd ones,  $A_{1,2}$ , wherein an increasing numerical label represents an heavier state.) Moreover, we assume the  $A_1$  to be produced via the decay of a heavy scalar Higgs boson of the model, the latter induced by  $gg$  fusion. (As finally established in [2], although some scope was demonstrated for single  $A_1$  production in association with a  $b\bar{b}$  prior to LHC Higgs data [3], this channel no longer carries any promise. Also, note that the scope of Vector Boson Fusion (VBF) and Higgs-strahlung is also currently being re-assessed in the light of the same experimental results [4].) In particular, we include the two intermediate channels  $A_1A_1$  and  $A_1Z$  while the decaying heavier Higgs boson can be any of the three neutral scalars.  $A_1$ 's thus produced decay into either  $b\bar{b}$  or (fully hadronic)  $\tau^+\tau^-$  pairs. The former decay is always the dominant one as the ratio of the branching ratios (BRs) for these modes is given approximately by the ratio of the  $b$  and the  $\tau$  masses squared, but the latter decay can be equally important due to a relatively smaller  $\tau^+\tau^-$  background. In case of the  $A_1Z$  decay channel, we only consider the leptonic ( $e^+e^-$  and  $\mu^+\mu^-$ ) decays of the  $Z$  boson.

To study the prospects for the discovery of an  $A_1$  at the LHC in all these production and decay channels, we employ hadron level Monte Carlo (MC) simulations. We perform a detailed signal-to-background analysis for each process of interest, employing jet substructure methods for detecting the  $b$  quarks originating from an  $A_1$  decay, assuming two  $b$ -tags in either two single  $b$ -jets or one fat  $b$ -jet. In particular, notice that, in case of a decaying SM-like Higgs state, the mass measurement of  $\sim 125$  GeV serves as an important kinematical handle for all signatures. Removing this condition reduces the sensitivity by a factor of 2 to 3. To recap, the  $A_1A_1$  pair thus produced decays into the  $b\bar{b}b\bar{b}$  ( $4b$ ),  $b\bar{b}\tau^+\tau^-$  ( $2b2\tau$ ) and  $\tau^+\tau^-\tau^+\tau^-$  ( $4\tau$ ) final state combinations while in the case of  $A_1Z$  production we will be looking at  $b\bar{b}\ell^+\ell^-$  ( $2b2\ell$ ) and  $\tau^+\tau^-\ell^+\ell^-$  ( $2\tau2\ell$ ), wherein  $\ell = e, \mu$ .

### II. MODEL SETUP AND SCANS

In order to remedy the proliferation of parameters typical of realistic models of Supersymmetry (SUSY), one usually invokes some kind of unification of these at high energy scales, typical of GUTs. However, as noted in [5], the fully constrained NMSSM (where all scalar and fermion masses as well as dimensionful couplings are unified, respectively, into three separate parameters) struggles to achieve the correct mass for the assumed SM-like Higgs boson, particularly in the presence of the latest theoretical and experimental constraints. In order to bypass this, the strict unification conditions mentioned above need to be relaxed. In a partially unconstrained version of the NMSSM the soft masses of the Higgs fields,  $m_{H_u}$ ,  $m_{H_d}$  and  $m_S$ , are taken as independent (from

TABLE I: The CNMSSM-NUHM input parameters and their scanned ranges.

Parameter	$m_0$ (GeV)	$m_{1/2}$ (GeV)	$A_0$ (GeV)	$\mu_{\text{eff}}$ (GeV)
Range	200 – 2000	100 – 1000	–3000 – 0	100 – 200
$\tan\beta$	$\lambda$	$\kappa$	$A_\lambda$ (GeV)	$A_\kappa$ (GeV)
1 – 6	0.4 – 0.7	0.01 – 0.7	–500 – 500	–500 – 500

$m_0$ ) parameters at the GUT scale. Through the minimisation conditions of the Higgs potential these three soft masses can then be traded at the Electro-Weak (EW) scale for the parameters  $\kappa$ ,  $\mu_{\text{eff}}$  and  $\tan\beta$ . Similarly, the soft trilinear coupling parameters  $A_\lambda$  and  $A_\kappa$ , though still input at the GUT scale, are also taken as independent (from  $A_0$ ). The model is thus defined in terms of the following nine continuous input parameters:

$$m_0, m_{1/2}, A_0, \tan\beta, \lambda, \kappa, \mu_{\text{eff}}, A_\lambda, A_\kappa,$$

where  $\tan\beta \equiv v_u/v_d$ , with  $v_u$  being the Vacuum Expectation Value (VEV) of the  $u$ -type Higgs doublet and  $v_d$  that of the  $d$ -type one. This version of the model serves as a good approximation of the most general EW-scale NMSSM as far as the Higgs sector dynamics is concerned. We, therefore, adopt it here to analyse the phenomenology of the light pseudoscalar and we refer to it as the CNMSSM-NUHM, where NUHM stands for Non-Universal (soft) Higgs Masses.

We scanned the CNMSSM-NUHM parameter space given in Tab. I to search for points giving  $m_{A_1} \lesssim 150$  GeV. We used the publicly available package NMSSMTools-v4.2.1 [6] for computation of the mass, coupling and BR spectrum of the Higgs bosons for each model point. In our scans we imposed the following constraints from  $b$ -physics, based on [7], and dark matter relic density measurements, from [8], as

- $\text{BR}(B_s \rightarrow \mu^+ \mu^-) = (3.2 (\pm 10\% \text{ theoretical error}) \pm 1.35) \times 10^{-9}$ ,
- $\text{BR}(B_u \rightarrow \tau \nu) = (1.66 \pm 0.66 \pm 0.38) \times 10^{-4}$ ,
- $\text{BR}(\bar{B} \rightarrow X_s \gamma) = (3.43 \pm 0.22 \pm 0.21) \times 10^{-4}$ ,
- $\Omega_\chi h^2 < 0.131$  ( $0.119 + 10\% \text{ theoretical error}$ ).

Exclusion limits from the LEP and LHC Higgs boson searches were also tested against using the HiggsBounds-v4.1.3 [9] package. Finally, from NMSSMTools we obtained the signal rates of the  $H_{\text{SM}}$  state, defined for a given decay channel  $X$  as

$$R_X \equiv \frac{\sigma(gg \rightarrow H_2) \times \text{BR}(H_i \rightarrow X)}{\sigma(gg \rightarrow h_{\text{SM}}) \times \text{BR}(h_{\text{SM}} \rightarrow X)}, \quad (1)$$

where  $h_{\text{SM}}$  is the true SM Higgs boson, which we required (for  $X = \gamma\gamma, ZZ$ ) to lie within the measured  $\pm 1\sigma$  ranges of the corresponding experimental quantities

$$\mu_{\gamma\gamma} = 1.13 \pm 0.24, \quad \mu_{ZZ} = 1.0 \pm 0.29 \quad \text{and} \quad (2)$$

$$\mu_{\gamma\gamma} = 1.57_{-0.28}^{+0.33}, \quad \mu_{ZZ} = 1.44_{-0.35}^{+0.40}, \quad (3)$$

provided by the CMS [10] and ATLAS [11] collaborations, respectively. The red and blue points in the forthcoming figures are the ones for which the calculated  $R_X$  lies within the range of  $\mu_X$  measured by CMS and ATLAS, respectively, while the green points are the ‘unfiltered’ ones for which neither of these two constraints are satisfied.

### III. SIGNAL-TO-BACKGROUND ANALYSIS

Following the scans, we carried out a dedicated signal-to-background analysis based on MC event generation for  $pp$  collisions at 14 TeV and variable integrated luminosity, for each process of interest. Using the program SuSHi-v1.1.1 [12], we first calculated the  $gg$  fusion production cross section of a SM Higgs boson with the same mass as that of our  $H_i$ . This cross section was then rescaled using the  $ggH_i$  reduced coupling in the

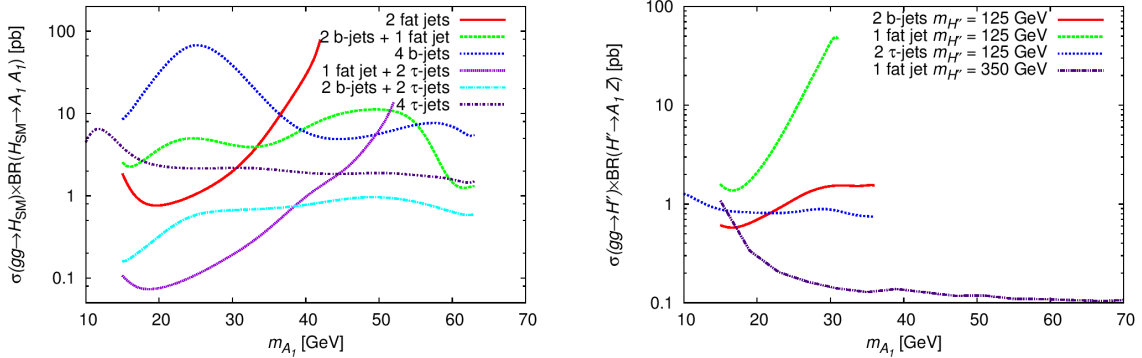


FIG. 1: Expected experimental sensitivities as functions of  $m_{A_1}$  in various possible final state combinations for (a)  $gg \rightarrow H_{\text{SM}} \rightarrow A_1 A_1$  and (b)  $gg \rightarrow H_i \rightarrow A_1 Z$ .

NMSSM and multiplied by the relevant BRs of the  $H_i$ 's, all of which are obtained from NMSSMTools. The backgrounds, which include  $pp \rightarrow 4b$ ,  $pp \rightarrow 2b2\tau$ ,  $pp \rightarrow 4\tau$ ,  $pp \rightarrow Z2b$  and  $pp \rightarrow Z2\tau$ , were computed with MadGraph5\_aMC@NLO [13]. Both signal and background for each process were hadronised and fragmented using Pythia 8.180 [14] interfaced with FastJet-v3.0.6 [15] for jet clustering. The parton-level acceptance cuts used in the event generation in MadGraph are: (i)  $|\eta| < 2.5$  and  $p_T > 15$  GeV for all final state objects; (ii)  $\Delta R \equiv \sqrt{(\Delta\eta)^2 + (\Delta\phi)^2} > 0.2$  for all  $b$ -quark pairs; (iii)  $\Delta R > 0.4$  for all other pairs of final state objects (where  $p_T$ ,  $\eta$ ,  $\phi$  are the transverse momentum, pseudorapidity and azimuthal angle, respectively).

As intimated, our use of the jet substructure method [16] implies that we have three possible signatures for a decaying  $A_1$ : one fat jet, two single  $b$ -jets and two  $\tau$ -jets. The fat jet analysis, which assumes boosted  $b$ -quarks, allows one to obtain much higher sensitivities, particularly for large masses of the decaying Higgs bosons. Notice that a key ingredient of this selection is the retention of two  $b$ -tags in both cases of a single fat  $b$ -jet and two slim  $b$ -jets. Failing this, i.e., if only one  $b$ -jet were to be tagged instead, the list of backgrounds would dramatically increase, in the form of QCD processes also including light-quark and gluon jets.

In general, we see in Fig. 1(b) that the fat jet analysis can be very effective when the  $A_1$  is much lighter than the  $H_i$  ( $i = 1, 2, 3$ ), but gets worse as  $m_{A_1}$  increases and, in fact, soon becomes relatively useless (the corresponding curves are thus cut off at the mass above which the analysis becomes ineffective). This is due to the fact that the fat jet analysis assumes boosted  $b$ -quark pairs. One can also see (especially in the curve with  $m_{H'} = 350$  GeV; hereafter  $H''$  refers to any of the three CP-even Higgs state directly produced in  $gg$  fusion while  $H'$  refers to the two states other than the  $H_{\text{SM}}$  in a given case) that, if the  $A_1$  mass becomes too small compared to the  $H_i$  mass, the sensitivity diminishes due to the  $b$ -jets becoming too collinear to be separable even with jet substructure methods. In the upper end, the cut-offs (for sensitivity curves other than those relying on the fat jet analysis) are determined by the kinematical upper limit for the given channel, i.e.,  $m_{A_1} \approx 62.5$  GeV for  $H_{\text{SM}} \rightarrow A_1 A_1$  and  $m_{A_1} \approx 35$  GeV for  $H_{\text{SM}} \rightarrow A_1 Z$ .

We finally calculated the expected cross sections for the signal processes which yield  $S/\sqrt{B} > 5$  for three benchmark accumulated luminosities at the LHC,  $\mathcal{L} = 30/\text{fb}$ ,  $300/\text{fb}$  and  $3000/\text{fb}$ , in various final state combinations, as functions of  $m_{A_1}$ . Notice that, in order to keep the figures readable, in the following section we will only show the curves corresponding to the analyses with the highest sensitivities for a given channel.

#### IV. RESULTS

In the NMSSM,  $H_1$  and  $H_2$  can both have masses around 125 GeV and SM-like properties, thereby alternatively playing the role of  $H_{\text{SM}}$ . A SM-like  $H_1$  with mass around 125 GeV can be obtained over wide regions of the CNMSSM-NUHM parameter space defined above. However, the additional requirement of  $m_{A_1} \lesssim 150$  GeV significantly changes this picture. In Fig. 2(a) we show the distribution of the mass of  $H_1$  against that of  $A_1$  for the points obtained in our scans assuming  $H_{\text{SM}} = H_1$ . We allow a rather wide range of  $m_{H_{\text{SM}}}$ , 122 GeV – 129 GeV, in order to take into account the experimental as well possibly large theoretical uncertainties in its model prediction. The heat map in the figure corresponds to the parameter  $\tan\beta$ . One can see a particularly dense population of points for  $\tan\beta \sim 1 - 6$  in the figure, with the mass of  $H_1$  reaching comparatively larger values than elsewhere. However,  $m_{A_1}$  for such points almost never falls below  $\sim 60$  GeV. In Fig. 2(b) we show  $m_{H_1}$

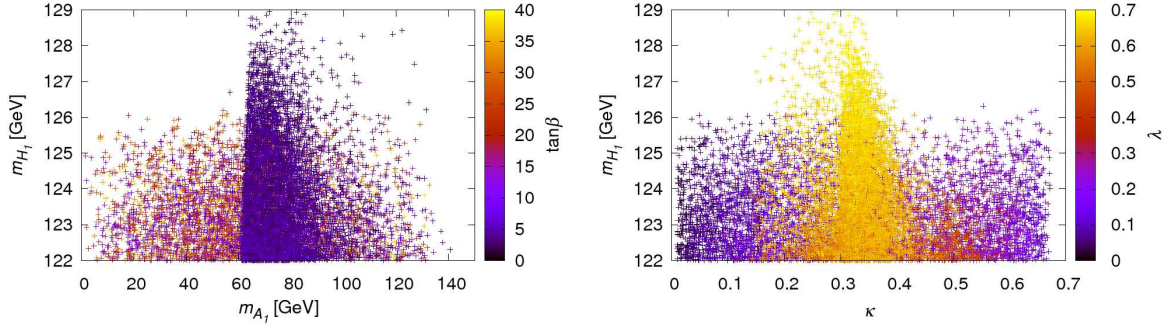


FIG. 2: Case with  $H_{\text{SM}} = H_1$ : (a) Mass of  $H_1$  vs. that of  $A_1$ , with the heat map showing the distribution of  $\tan\beta$ ; (b)  $m_{H_1}$  as a function of the parameter  $\kappa$ , with the heat map showing the distribution of the coupling  $\lambda$ .

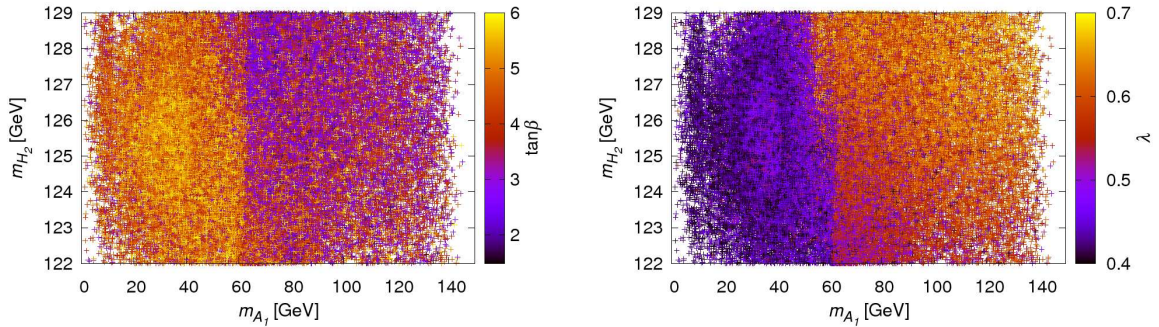


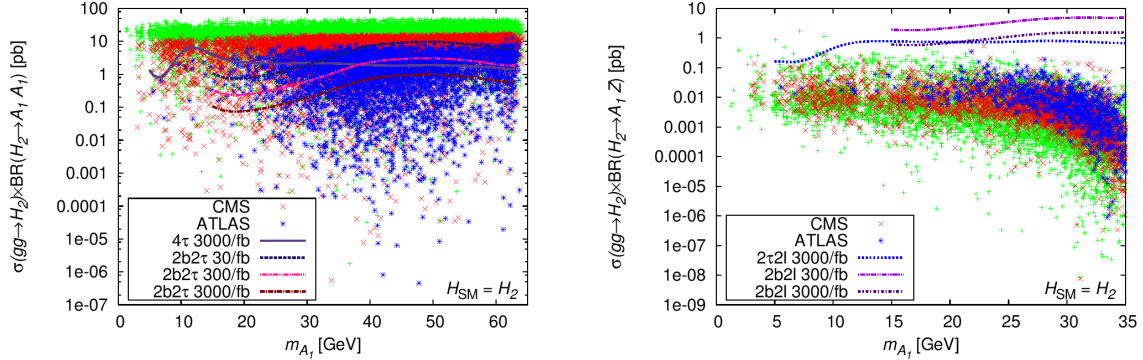
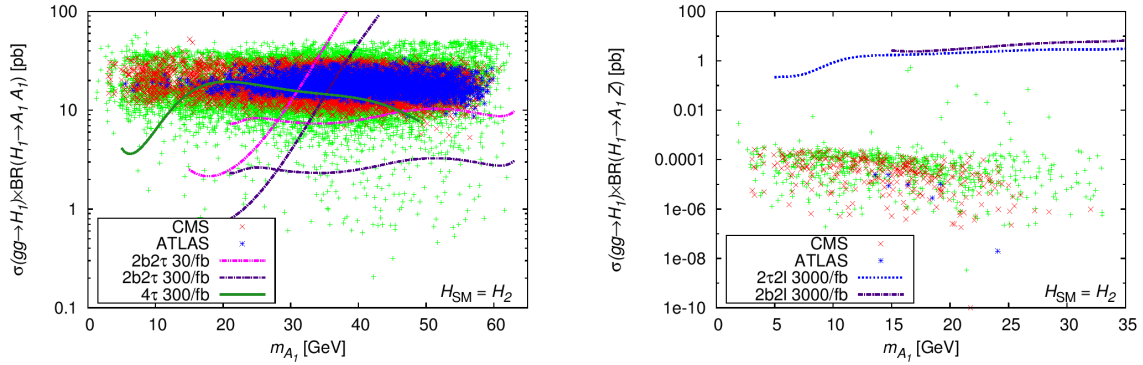
FIG. 3: Mass of  $H_2$  vs. that of  $A_1$  for the case with  $H_{\text{SM}} = H_2$ . The heat map shows (a) the distribution of  $\tan\beta$  and (b) the distribution of  $\lambda$ .

as a function of the coupling  $\kappa$ , with the heat map corresponding to the coupling  $\lambda$ . Again there is a clear strip of points with  $\lambda \gtrsim 0.6$  (and  $\kappa \sim 0.15 - 0.5$ ) for which  $m_{H_1}$  can be as high as 129 GeV. The rest of the points, corresponding to smaller  $\lambda$  and larger  $\tan\beta$ , can barely yield  $m_{H_1}$  in excess of 126 GeV. The reason for the behaviour of  $m_{H_1}$  observed in these figures is well explained in Ref. [2] and is essentially attributable to the expression of  $m_{H_1}$  in terms of the CNMSSM-NUHM input parameters.

Figs. 3(a) and (b) show that  $H_2$  with a mass lying in the entire allowed range can be obtained much more easily without always requiring very low  $\tan\beta$  or very large  $\lambda$ . Moreover, the corresponding parameter space points can also yield fairly small  $A_1$  (with sizeable  $\text{BR}(H_2 \rightarrow A_1 A_1/Z)$ ), without the  $H_2$  deviating too much from the LHC Higgs boson signal rate measurements. We will, therefore, concentrate in the remainder of this report only on the  $H_2$  solution for  $H_{\text{SM}}$  (i.e.,  $H_{\text{SM}} = H_2$ ).

#### A. Production via $H_{\text{SM}} \rightarrow A_1 A_1/Z$

In Fig. 4(a) we show the prospects for the  $H_2 \rightarrow A_1 A_1$  channel when  $H_2$  is SM-like. We see that, compared with the  $H_{\text{SM}} = H_1$  case, a much larger part of the parameter space can be probed at the LHC, even at as low as 30/fb of integrated luminosity. The reason is clearly that in this case the points with  $m_{A_1} < m_{H_{\text{SM}}}/2$  belong to the parameter space regions where  $\text{BR}(H_2 \rightarrow A_1 A_1)$  is indeed sufficiently enhanced without causing the  $H_{\text{SM}}$  for these points to depart from a SM-like behaviour. This is also the reason why a large fraction of the points with large event rates is consistent also with the CMS and ATLAS measurements of  $\mu_{\gamma\gamma/ZZ}$ . In Fig. 4(b) we see instead that the prospects in the  $H_2 \rightarrow A_1 Z$  channel are poor.


 FIG. 4: Total cross sections for  $H_{\text{SM}} = H_2$  for (a)  $gg \rightarrow H_{\text{SM}} \rightarrow A_1 A_1$  and (b)  $gg \rightarrow H_{\text{SM}} \rightarrow A_1 Z$ .

 FIG. 5: Total cross sections for  $H_{\text{SM}} = H_2$  for (a)  $gg \rightarrow H_1 \rightarrow A_1 A_1$  and (b)  $gg \rightarrow H_1 \rightarrow A_1 Z$ .

### B. Production via $H' \rightarrow A_1 A_1 / Z$

The prospects for the discovery of a light pseudoscalar in the  $H_1 \rightarrow A_1 A_1$  and  $H_1 \rightarrow A_1 Z$  decay channels, for a singlet-like  $H_1$ , are illustrated in Figs. 5(a) and (b), respectively. One sees in Fig. 5(a) that almost all the points complying with the current CMS and/or ATLAS constraints on  $R_X$  are potentially discoverable, even at  $\mathcal{L} = 30/\text{fb}$ . Thus a large part of the scanned NMSSM parameter space can be probed via this decay channel. In particular, since such light pseudoscalars cannot easily be obtained for the case with  $H_{\text{SM}} = H_1$ , it should essentially be possible to exclude or confirm  $m_{A_1} \lesssim 60$  GeV in the NMSSM at the LHC via this channel. Note also that such an exclusion will not cover the narrow regions of parameter space where  $m_{A_1} > m_{H_1}/2$ . Finally, in Fig. 5(b), we see that the prospects for the discovery of  $A_1$  via the  $H_1 \rightarrow A_1 Z$  channel are non-existent.

For the decay chain starting from  $H_3$ , the situation is illustrated in Fig. 6(a), where we see that the  $H_3 \rightarrow A_1 A_1$  channel is inaccessible also due to the fact that, for such high masses of  $H_3$  ( $\gtrsim 400$  GeV), the production cross section gets diminished. Moreover, other decay channels of  $H_3$  dominate. Conversely, the  $H_3 \rightarrow A_1 Z$  channel, shown in Fig. 6(b), shows much more promise. This has to do with the increased sensitivity in the fat jet analysis when the involved masses are high as well as the relatively large  $H_3 A_1 Z$  coupling, which is actually somewhat larger here than in the  $H_{\text{SM}} = H_1$  case, due to a correspondingly larger doublet component of  $A_1$ . We therefore emphasise again that this channel will be an extremely important probe for an NMSSM  $A_1$  with mass greater than  $\sim 60$  GeV.

## V. SUMMARY

We have found that the decays of the NMSSM CP-even scalars, including in particular the SM-like Higgs boson, whether  $H_1$  or  $H_2$ , carry the potential to reveal an  $A_1$  with mass  $\lesssim 60$  GeV for an integrated luminosity at the LHC as low as 30/fb. This is particularly true when the SM-like Higgs state is the  $H_2$ . Most notably

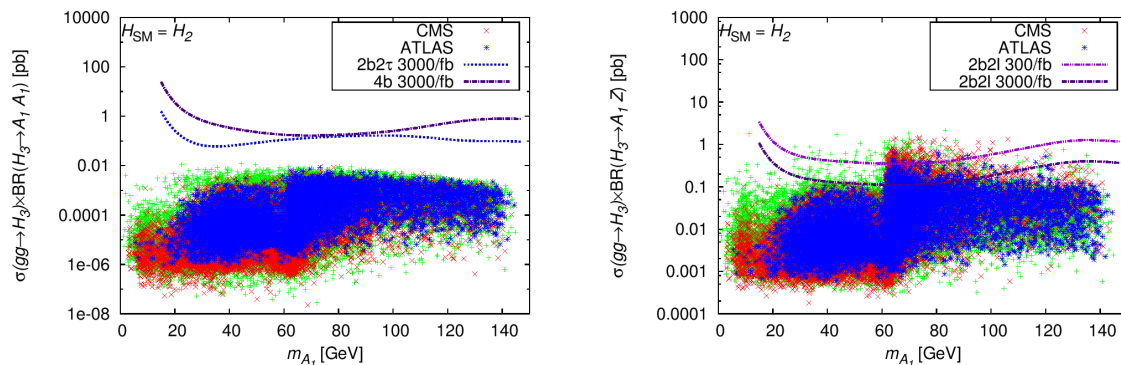


FIG. 6: Total cross sections for  $H_{\text{SM}} = H_2$  for (a)  $gg \rightarrow H_3 \rightarrow A_1 A_1$  and (b)  $gg \rightarrow H_3 \rightarrow A_1 Z$ .

though, when the  $A_1$  is heavier than  $\sim 60$  GeV, while its pair production via decays of the two lightest CP-even Higgs bosons becomes inaccessible, the  $gg \rightarrow H_3 \rightarrow A_1 Z$  channel takes over as the most promising one. This (hitherto neglected) mode is, therefore, of great importance and warrants dedicated probes in future analyses at the LHC.

Such results are based upon parton-level MC event generation supplemented by parton shower and hadronisation. Hence, final validation of our results can be done through a proper detector simulation. A key aspect of this would be the implementation of double  $b$ -tagging throughout.

### Acknowledgments

This work has been funded in part by the Welcome Programme of the Foundation for Polish Science. S. Moretti is financially supported in part through the NExT Institute and further acknowledges funding from the Japan Society for the Promotion of Science (JSPS) in the form of a Short Term Fellowship for Research in Japan (Grant Number S14026). He is also grateful to the Theoretical Physics Group at the Department of Physics of the University of Toyama for their kind hospitality during the tenure of the JSPS award. S. Munir is supported in part by the Swedish Research Council under contracts 2007-4071 and 621-2011-5107. L. Roszkowski is also supported in part by an STFC consortium grant of Lancaster, Manchester and Sheffield Universities. The use of the CIS computer cluster at NCBJ is gratefully acknowledged.

- 
- [1] U. Ellwanger, C. Hugonie and A. M. Teixeira, Phys. Rept. **496**, 1 (2010).
  - [2] N. E. Bomark, S. Moretti, S. Munir and L. Roszkowski, JHEP **1502**, 044 (2015).
  - [3] M. M. Almarashi and S. Moretti, arXiv:1205.1683 [hep-ph].
  - [4] N. E. Bomark, S. Moretti and L. Roszkowski, in preparation.
  - [5] K. Kowalska, S. Munir, L. Roszkowski, E. M. Sessolo, S. Trojanowski et al., Phys. Rev. D **87**, 115010 (2013).
  - [6] <http://www.th.u-psud.fr/NMHDECAY/nmssmtools.html>.
  - [7] Particle Data Group Collaboration, Phys. Rev. D **86**, 010001 (2012).
  - [8] Planck Collaboration, Astron. Astrophys. **571**, A16 (2014).
  - [9] P. Bechtle, O. Brein, S. Heinemeyer, O. Stal, T. Stefaniak et al., Eur. Phys. J. C **74**, 2693 (2014).
  - [10] CMS Collaboration, CMS-PAS-HIG-14-009.
  - [11] ATLAS Collaboration, ATLAS-CONF-2014-009.
  - [12] R. V. Harlander, S. Liebler and H. Mantler, Comp. Phys. Commun. **184**, 1605 (2013).
  - [13] J. Alwall, R. Frederix, S. Frixione, V. Hirschi, F. Maltoni, et al., JHEP **1407**, 079 (2014).
  - [14] T. Sjostrand, S. Mrenna and P. Z. Skands, Comput. Phys. Commun. **178**, 852.
  - [15] M. Cacciari, G. P. Salam and G. Soyez, Eur. Phys. J. C **72**, 1896 (2012).
  - [16] J. M. Butterworth, A. R. Davison, M. Rubin and G. P. Salam, Phys. Rev. Lett. **100**, 242001 (2008).